ACS OMEGA

http://pubs.acs.org/journal/acsodf

Article

Long-Lasting Proteinaceous Nanoformulation for Tumor Imaging and Therapy

Lai Zhao, Xinquan Gu,* Fuquan Jiang,* Bo Li, Shuang Lu, Fan Wang, Yao Sun,* Kai Liu, and Jingjing Li*

Cite This: *ACS Omega* 2022, 7, 31299−31308

Read Online

ACCESS | Metrics & More | Article Recommendations | Supporting Information

ABSTRACT: Nanodrugs have attracted increasing interest in drug delivery and disease treatment. However, the cumbersome preparation process and the poor biocompatibility of nanodrugs obstruct their clinical translation. In this study, we utilized a self-assembly strategy to develop a low-toxicity, long-lasting nanodrug for the effective treatment and real-time monitoring of bladder tumors. The accurate self-assembly of compatible raw materials allowed for an encapsulation rate of 43.7% for insoluble erdafitinib. Interestingly, robust therapeutic effects and reduced side effects could be realized simultaneously using this nanodrug, enabling broader scenarios for the clinical application of erdafitinib. Furthermore, the nanodrug exhibited a significantly prolonged *in vivo* half-life (14.4 h) and increased bioavailability (8.0 μg/mL·h), which were 8.3 times and 5.0 times higher than those of its nonformulated counterpart. Also, it is worth mentioning that the introduction of a fluorescent protein module into the nanodrug brought up a novel possibility for real-time feedback on the therapeutic response. In conclusion, this research revealed a versatile technique for developing low-toxicity, long-acting, and multifunctional nanoformulations, paving the way for multidimensional therapy of malignant tumors.

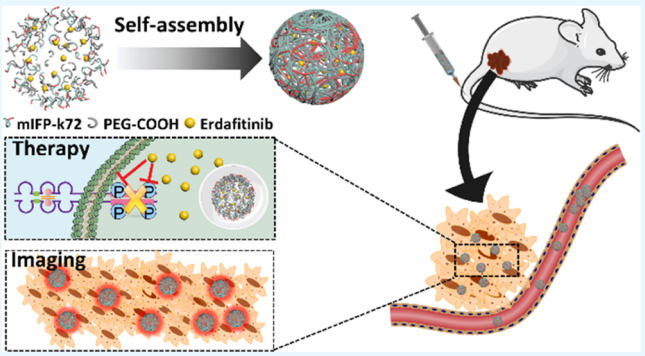

INTRODUCTION

Bladder cancer is documented as the 10th most common malignant tumor worldwide, accounting for nearly 210,000 deaths each year.[1,2] Surgical resection, chemotherapy, and radiotherapy remain the first-line treatments for bladder cancers. However, these treatments have been extensively criticized for their tremendous and indiscriminate damage to normal cells and tissues.[3] In recent years, targeted therapy and immunotherapy are emerging as available options for bladder cancer treatment.[3,4] Notably, erdafitinib is the first pan-fibroblast growth factor receptor (FGFR) inhibitor to be approved for the targeted treatment of advanced or metastatic urothelial carcinoma by the US Food and Drug Administration, and it demonstrates a selective and potent therapeutic effect.[5,6] However, poor compliance with daily administration and the frequent side effects, such as hyperphosphatemia and eye disorders, undoubtedly restrict its clinical applications.[7,8] Therefore, it is imperative to develop a novel formulation characterized by robust therapeutic efficacy, safety, and better pharmacokinetics for the effective treatment of bladder cancer.

Nanodrugs hold a lot of promise when it comes to the delivery and functionalization of medication.[9−13] Through precise design, nanoparticles could be afforded with different functions, such as enhanced drug solubility, targeted drug delivery, controlled drug release, improved pharmacokinetics (PK), etc.[14−17] Specifically, nanoparticles that possess both fluorescence and therapeutic effects could help accomplish simultaneous tumor suppression and surveillance, which is urgently needed for malignant tumor treatment.[18−20] Real-time feedback of the therapeutic response promotes quick adjustment of therapy regimens, thereby ensuring the effective treatment of advanced cancers. Therefore, these nanoparticles are ideal for the treatment of bladder cancer, which is highly prone to recurrence and progression. Nevertheless, the employment of organic or inorganic materials in such nanoparticles led to some unavoidable problems, such as non-biodegradability, poor biocompatibility, and toxicity.[21−24] In addition, the effective production of nanodrugs cannot be reliably guaranteed because of the complex preparation process and wide particle size distribution.[25] More importantly, the clinical translation of nanodrugs may be restricted by many aspects, for instance, low drug penetration and systemic toxicity from byproducts.[26−28] Thus, the development of

Received: June 7, 2022
Accepted: August 12, 2022
Published: August 24, 2022

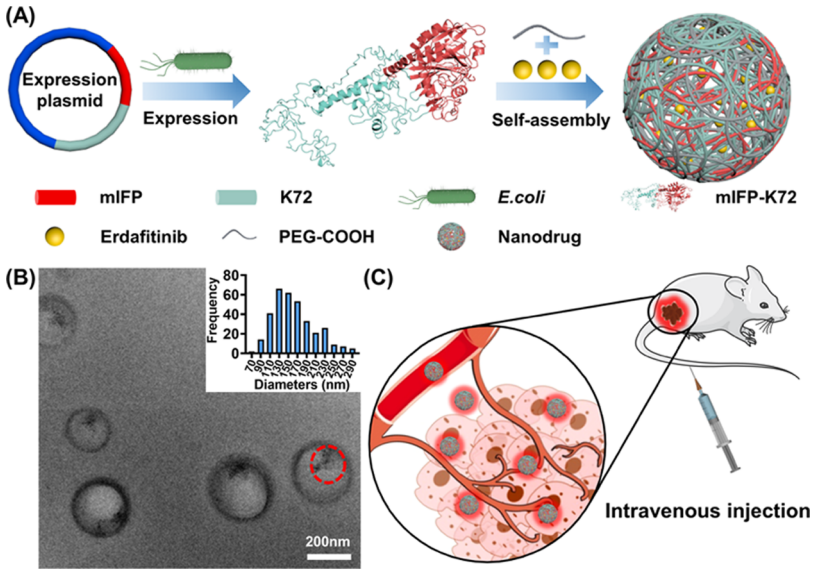

Figure 1. Preparation and characterization of the nanodrug. (A) Schematic illustration of the nanodrug preparation. The recombinant plasmid was constructed and transformed into *E. coli* for the expression of the chimeric protein mIFP-K72. mIFP-K72, PEG-COOH, and erdafitinib could precisely self-assemble into spherical nanoparticles. (B) Transmission electron microscopy of the nanodrug revealed that it presented a uniform spherical structure with a diameter of ∼160 nm. The dark dot in the red circle indicates clusters of encapsulated erdafitinib. The scale bar is 200 nm. (C) Nanodrugs spontaneously accumulated in tumor sites via the enhanced permeability and retention (EPR) effect after being injected into the circulation and demonstrated both therapeutic and imaging effects.

tailored nanodrugs for bladder cancer treatment in a safe, simple, and reproducible way remains elusive.

In this study, we rationally designed and prepared a protein-based nanodrug for effective bladder tumor treatment. By employing biocompatible raw materials and a precise self-assembly strategy, we successfully prepared a customized nanodrug that presented low toxicity, high loading efficiency, and sustained release of erdafitinib, which significantly inhibited tumor growth. Specifically, a nanocarrier was developed through electrostatic interactions between the cationic chimeric protein and the anionic polyethylene glycol, presenting a spherical structure with a hydrophobic central cavity, which was highly suitable for the protection and encapsulation of hydrophobic drugs. Notably, the nanodrug exhibited a prolonged *in vivo* half-life (14.4 h) and increased bioavailability (8.0 μg/mL·h), which were 8.3 times and 5.0 times higher than those of pure erdafitinib, respectively. Furthermore, the dosing frequency and side effects of erdafitinib were significantly reduced in the nanodrug-treated models. In addition, the nanodrug also permitted highly sensitive imaging, which allowed the diagnosis and real-time monitoring of the therapeutic response of bladder tumors. In general, we successfully prepared a multifunctional nanodrug through a simple self-assembly approach, which brought up new opportunities for the future generation and reproduction of low-toxicity, long-lasting, and robust nanodrugs as well as the comprehensive treatment of malignant tumors.

RESULTS AND DISCUSSION

Erdafitinib-based nanodrugs were prepared by the self-assembly of three components, including a cationic chimeric protein, carboxylated polyethylene glycol (PEG-COOH), and a hydrophobic drug. To construct a multifunctional protein, coding sequences of elastin-like polypeptide (ELP) and monomeric near-infrared fluorescent protein (mIFP) were combined into one chimeric plasmid (Figure 1A). In the chimeric protein, the ELP segment consists of a repetitive pentapeptide unit of VPGKG, from which the lysine endows the chimeric protein with cationic characteristics and the mIFP segment could exhibit superb fluorescence-imaging capability.[18,29,30] The purity and molecular weight of the expressed mIFP-K72 (72 denotes the lysine content) were characterized by sodium dodecyl sulfate-polyacrylamide gel electrophoresis and matrix-assisted laser desorption/ionization time-of-flight mass spectrometry (Figure S1). As shown in Figure S2, the erdafitinib suspension turned transparent after precise self-assembly with the other two components, indicating the high drug-loading capacity of the nanocarrier. The drug-loading efficiency and encapsulation efficiency were 33.6 and 43.7%, respectively, which were much greater than the solubility of erdafitinib. According to the results of transmission electron microscopy (TEM), the vehicle (the nanoparticles formed by assembling mIFP-K72 with PEG-COOH) showed a hollow spherical structure, whereas clusters of the hydrophobic erdafitinib could be seen clearly in the interior cavity of the nanodrug (Figures 1B and S3). The spherical structure of the nanodrug was constructed by electrostatic interactions between cationic mIFP-K72 and anionic PEG-COOH, and erdafitinib was encapsulated via hydrophobic interactions. The average diameter of the nanodrug was 161.8 ± 45.6 nm, which was slightly larger than that of the vehicle (120.8 ± 36.1 nm) (Figures 1B and S3). Interestingly, PEG-COOH and erdafitinib could form solid nanoparticles with a diameter of 51.4 ± 14.1 nm (Figure S3C). It was easy to find that the addition of mIFP-K72 made the nanoparticles looser by comparing the diameters of these two nanoparticles. Therefore, mIFP-K72 plays an imperative role in maintaining the hollow structure of the nanodrug. Indeed, we proved that the sizes of protein−PEG nanoparticles can be manipulated by changing the polypeptide chain length of the protein,[18] and thus, mIFP-K72 allows a larger nanoparticle size and higher drug-loading capacity. In addition, the dynamic light scattering (DLS)

https://doi.org/10.1021/acsomega.2c03561
ACS Omega 2022, 7, 31299−31308

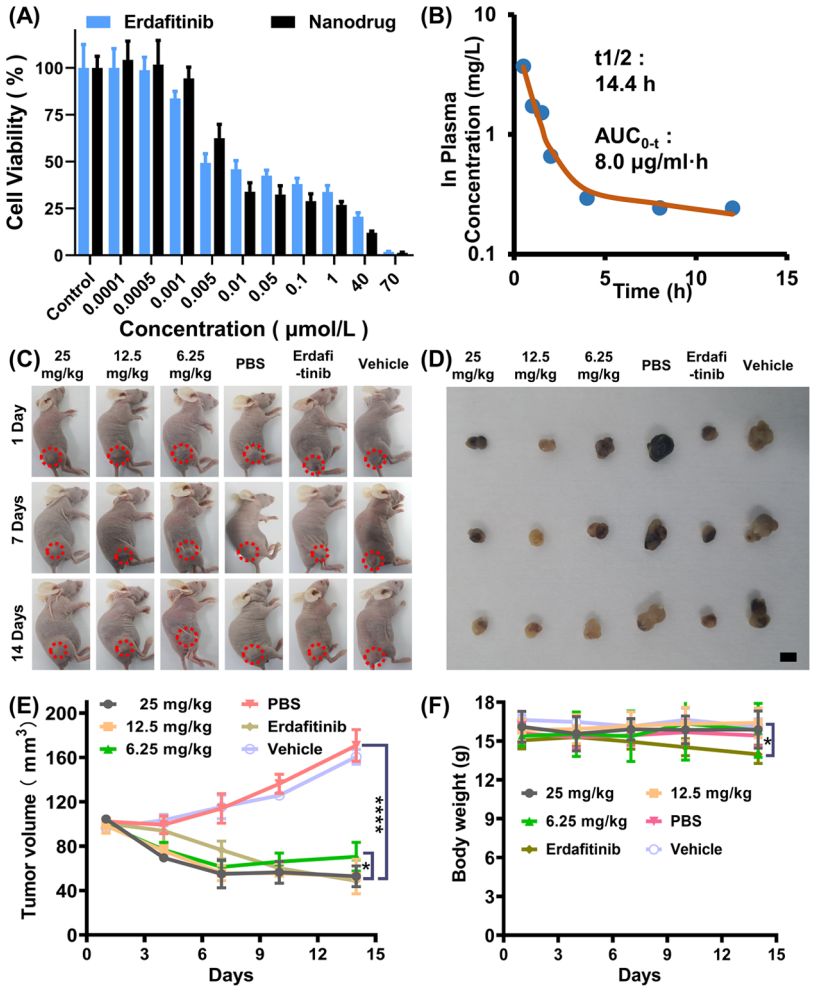

Figure 2. Evaluation of the anti-tumor effect and pharmacokinetic parameters of the nanodrug. (A) Cell viability of RT4 cells after incubation with erdafitinib or the nanodrug for 72 h. These two groups exhibited similar *in vitro* anti-tumor effects. (B) *In vivo* plasma concentration profile of the nanodrug revealed outstanding pharmacokinetic parameters. (C) Images of xenogeneic subcutaneous tumor models during the treatment. Obviously, the tumor growth was inhibited in the nanodrug and the erdafitinib groups, whereas the tumors grew rapidly in the PBS and the vehicle groups. The dashed red circles represent tumor sites. (D) Isolated tumors of xenografted tumor models after 2 weeks of treatment. The scale bar is 5 mm. (E) Tumor volumes of mice models during the treatment. The tumor volume of the 25 mg/kg group was significantly lower than that of the 6.25 mg/kg group or the PBS group (*$p < 0.05$, ****$p < 0.0001$). (F) Body weight variations of mice models in each group. Body weight loss was observed in the erdafitinib group, and there was a significant difference between the PBS and the erdafitinib groups (*$p < 0.05$).

revealed a larger diameter when compared with the results of TEM, which could be attributed to the hydrated state of the samples (Figure S4). However, the nanodrug and the vehicle displayed opposite trends of diameters in TEM and DLS. In the solvent state, erdafitinib could get protonated by trapping hydrogen ions of PEG-COOH. The protonated erdafitinib could interact with PEG-COO^- through electrostatic interactions, thus leading to a more compact structure. As a result, the diameter of the nanodrug is slightly smaller than that of the vehicle in DLS. After intravenous injection, the nanosized medicine accumulated and functioned at the tumor site, and the introduction of mIFP endowed it with the capacity to trace the nanocarrier, revealing a promising therapeutic strategy for tumors (Figure 1C).

To evaluate the *in vitro* anti-tumor effect of the nanodrug, a cytotoxicity assay and live/dead staining were carried out. As erdafitinib was reported to be a selective FGFR inhibitor, we employed two kinds of bladder cancer cells to validate its selectivity, where the RT4 cells were determined to overexpress FGFR3 and the T24 cells showed low expression of FGFR3.[31−33] The *in vitro* anti-tumor effect of pristine erdafitinib and the nanodrug were similar in RT4 cells (Figure 2A). Specifically, erdafitinib and the nanodrug exhibited half-maximal inhibitory concentrations (IC50) of 29.9 and 14.0 nmol/L, respectively, demonstrating that the assembly of erdafitinib hardly influenced its anti-tumor efficacy (Figure S5A,B). In contrast, erdafitinib and the nanodrug exhibited weaker anti-tumor effects in T24 cells, with IC50 values of 35.4 and 25.5 μmol/L, respectively, which verified the selectivity of erdafitinib (Figure S6A−C). Interestingly, the nanodrug was more effective than pristine erdafitinib, which could be attributed to the enhanced cellular internalization of nanoparticles.[34,35] Furthermore, the vehicle showed no significant cytotoxicity toward both RT4 and T24 cells (Figures S5C and S6C). The results of live/dead staining were consistent with that of the cytotoxicity assay, where only a few dead RT4/T24 cells could be observed in the phosphate-buffered saline (PBS) group and about half of the cells died following the treatment with erdafitinib or the nanodrug (Figure S7). In addition, the PK characteristics of the robust nanodrug were further

https://doi.org/10.1021/acsomega.2c03561
ACS Omega 2022, 7, 31299−31308

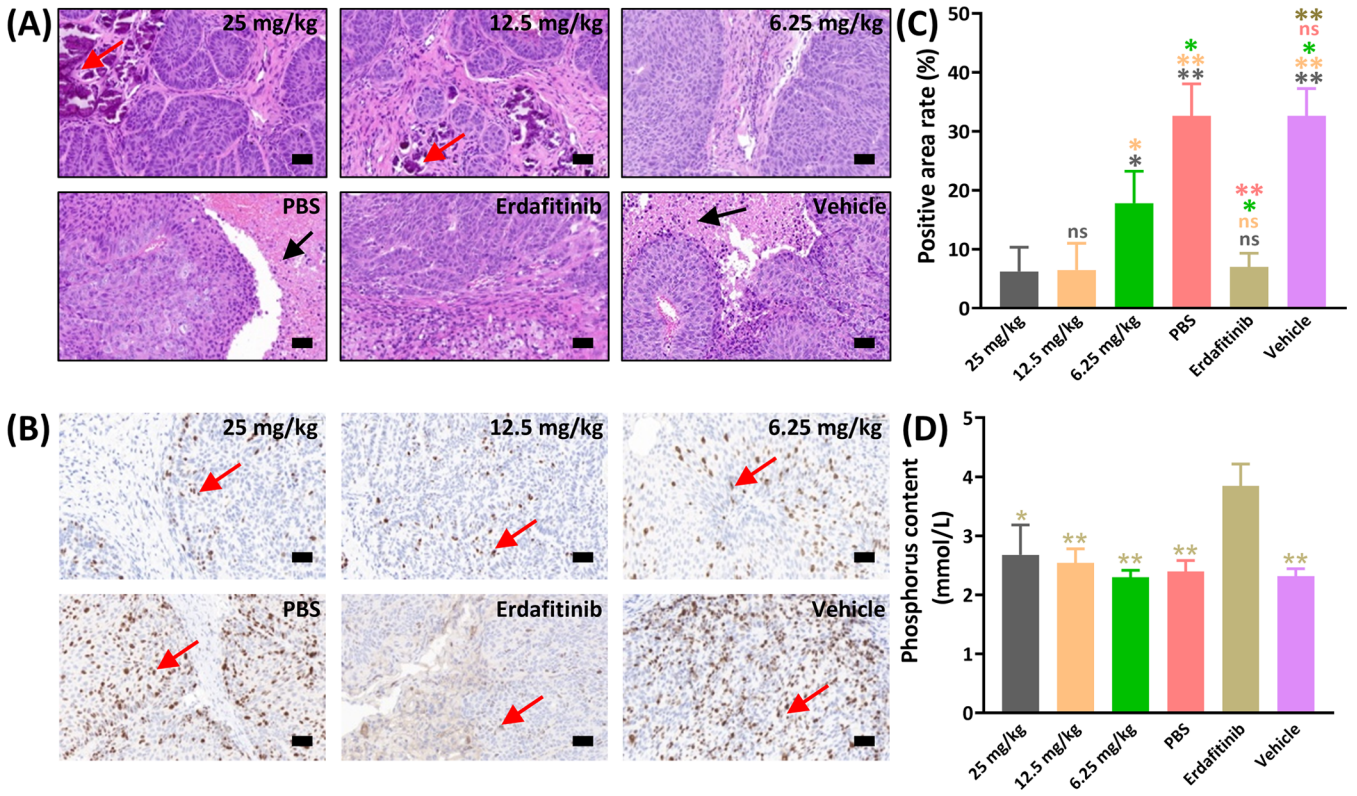

Figure 3. Histological assessment of the tumor tissue and evaluation of side effects of the nanodrug. (A) H&E staining of the tumor tissue. Most tumor cells were arranged in a mass, and the infiltration of tumor cells was significantly higher in the control groups. Calcification in the stroma was observed in the nanodrug-treated group (red arrows), whereas the control groups showed scattered necrosis areas (black arrows). The scale bar is 50 μm. (B) Immunohistochemical staining of Ki67. The Ki67 expressed in tumor cells were stained in brown (red arrows). The result revealed that drug-treated groups presented less Ki67 expression than the control groups. Interestingly, the 6.25 mg/kg group showed a lower Ki67 expression than the other three treatment groups, whereas there was no significant difference between the other three groups. The scale bar is 50 μm. (C) Quantification of Ki67 expressions showed a significant difference between the treatment groups and the control groups. The comparison was carried out in pairs: the color of the columns and the color of the symbols above the column represent the treatment groups (ns, no significant difference; *$p < 0.05$, ** $p < 0.01$). (D) Comparison of the plasma phosphorus content in each group. The erdafitinib group showed a higher plasma phosphorus content compared with the other groups (*$p < 0.05$, **$p < 0.01$).

assessed, and significantly improved PK parameters were observed. Specifically, when compared with the counterpart of pristine erdafitinib, the *in vivo* half-life and bioavailability (AUC) of the nanodrug increased by 8.3 times (14.4 h) and 5.0 times (8.0 μg/mL·h) in a mice model, respectively.[36] PEG-COOH is believed to play an irreplaceable role in protecting the nanodrug from plasma albumin absorption and clearance by the mononuclear phagocytic system, thereby allowing an increase in the blood circulation time and bioavailability.[37]

A xenogeneic subcutaneous model was employed to evaluate the *in vivo* anti-tumor effect of the nanodrug. After being successfully established, the models were randomly divided into six groups, including three nanodrug groups of different concentrations (25, 12.5, and 6.25 mg/kg group), PBS group, erdafitinib group, and vehicle group. All drugs were administrated by intravenous injection on days 1, 4, and 7, except for erdafitinib, which was given orally every day. During the treatment, the PBS and the vehicle groups exhibited rapid tumor growth, whereas the other groups showed significant inhibition of tumor growth. Notably, the 25 mg/kg, 12.5 mg/kg, and erdafitinib groups demonstrated similar tumor inhibition effects, with a final tumor volume of 50.0 mm^3. On the other hand, the tumor suppression in the 6.25 mg/kg group was weaker than that in the other three treatment groups (nanodrug groups and erdafitinib group), and there was a significant difference between the 6.25 mg/kg and the 25 mg/kg groups. In contrast, the control groups (PBS and vehicle groups) exhibited no anti-tumor effects with final tumor volumes of 170.7 and 160.5 mm^3, respectively (Figure 2C,E). The anti-tumor effect was further evaluated by the tumor growth inhibition (TGI) value; the TGI values for the 25, 12.5, and 6.25 mg/kg groups and the erdafitinib group were 69.1, 69.1, 58.6, and 71.4%, respectively. The corresponding tumor tissues are presented in Figure 2D. It is considered that the enhanced permeability and retention effect (EPR effect) as well as the prolonged *in vivo* half-life were responsible for the comparable therapeutic effects of the nanodrug even with a reduced dosage. Benefitting from the prolonged circulation time, more nanodrugs penetrated the tumor tissue through the defective vascular wall and were retained in the tumor site, finally showing a robust therapeutic effect. Besides, we carefully recorded the body weight variations of models during the treatments. Continuous body weight loss was observed in the erdafitinib group, indicating the systematic damage of pristine erdafitinib. The final average body weight of the erdafitinib group was significantly lower than those of the other groups (Figure 2F).

Histomorphology and Ki67 expression of tumor tissues were further investigated by hematoxylin and eosin (H&E) staining and immunohistochemistry. Apparently, more tumor cell

https://doi.org/10.1021/acsomega.2c03561
ACS Omega 2022, 7, 31299−31308

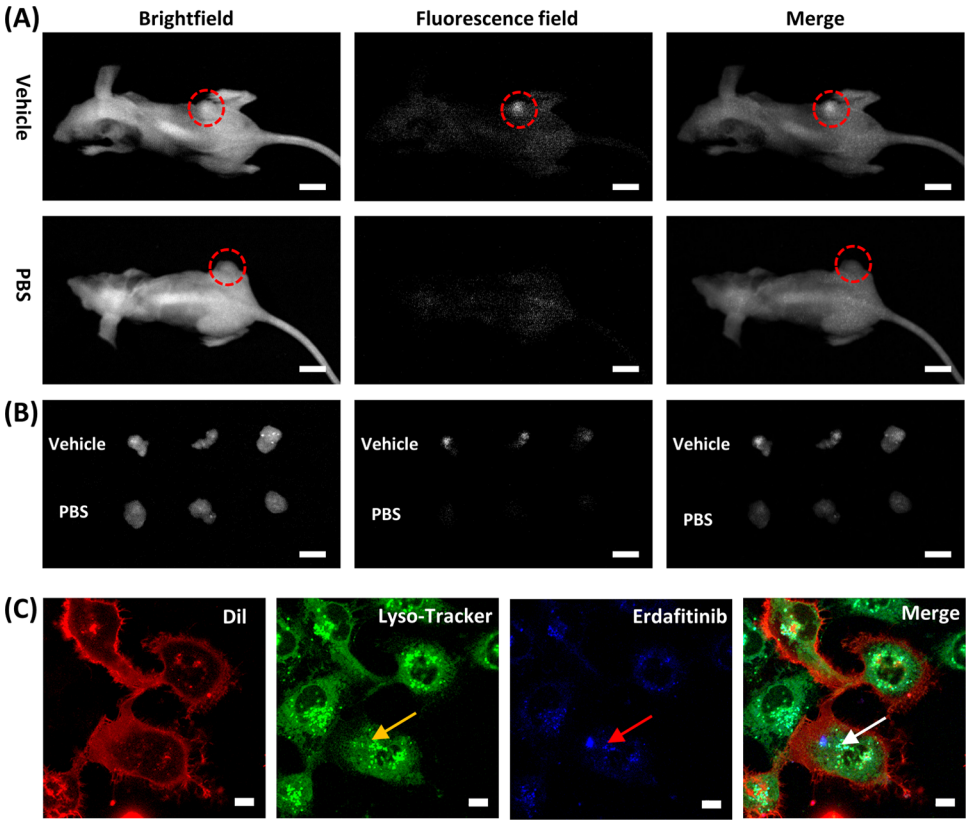

Figure 4. Investigation of the *in vivo* fluorescence imaging capability and intracellular distribution of the nanodrug. (A) Vehicle-treated models displayed bright fluorescence locally at the tumor site, whereas the control group exhibited no fluorescence. The scale bar is 1 cm; λ_{ex} = 665 nm and λ_{em} = 710 nm. (B) Fluorescence performance of the corresponding tumor tissues was consistent with that of the mice models. The scale bar is 1 cm. (C) Cell membranes and lysosomes were stained in red and green by Dil and Lyso-Tracker, respectively, and the erdafitinib inside the nanodrug showed a blue fluorescence after being excited. It should be noticed that the fluorescence signal of erdafitinib overlapped with that of the lysosome, suggesting that the nanodrug was mainly distributed in the lysosome. The yellow and red arrows point toward the fluorescence of lysosomes and erdafitinib, respectively, and the white arrow points toward the merged fluorescence signal. The scale bar is 10 μm.

infiltration and less mesenchymal tissue were seen in the control groups, which was in line with the rapid tumor growth in these two groups. In addition, scattered necrotic areas should also be noticed in these groups, which resulted from the fast growth of tumor tissues (Figure 3A). In contrast, calcification could be found in the 25 and 12.5 mg/kg groups, indicating a favorable prognosis for the tumor treatment. Ki67 is a nuclear antigen that plays a critical role in tumor cell proliferation. As shown in Figure 3B, treatment with erdafitinib or the nanodrug resulted in much lower Ki67 expression, revealing the potent therapeutic effects of these drugs. The quantification of Ki67 expression was further conducted for a more direct comparison. There was a distinct difference between the treatment groups and the control groups in Ki67 expression (Figure 3C). Interestingly, the 6.25 mg/kg group demonstrated medium Ki67 expression, which was consistent with the above results. In conclusion, the long-lasting nanodrug displayed potent *in vivo* anti-tumor effects and was promising to improve the compliance of patients due to its reduced dosage.

After the clinical administration of erdafitinib, many adverse events were documented to frequently emerge, such as nausea, diarrhea, and increased plasma phosphate levels.[8] Surprisingly, treatment with the nanodrug did not lead to weight loss in the tumor models. Furthermore, we detected the plasma phosphorus level in each group, and no significant increase could be found in the nanodrug groups, whereas the erdafitinib group showed a higher phosphorus content of 3.8 mmol/L (Figure 3D). Thus, this suggested that the application of the nanodrug effectively reduced the off-target side effects of erdafitinib. Patients may develop hyperphosphatemia after the administration of erdafitinib, which would lead to dose reduction or intermittent or permanent treatment interruption.[38] Therefore, this work developed a new strategy to mitigate the side effects of erdafitinib, which might open up the possibility for its broader clinical application.

Considering that the protein imaging agent was also encapsulated in the nanodrug, we further investigated its fluorescence imaging capability using a xenogeneic subcutaneous tumor model.[18] The chimeric protein was completely bound with the cofactor biliverdin before self-assembly with PEG-COOH, and there was no encapsulated erdafitinib. After 16 h of incubation, the fluorescent signal was detected via a Maestro (CRi) imaging system. The vehicle-treated models displayed bright fluorescence only at the tumor location, whereas the PBS-treated models showed no fluorescence (Figure 4A). In addition, the isolated tumor tissues exhibited similar results (Figure 4B). The strong targeted imaging performance should be attributed to the passive targeting of the vehicle and the high sensitivity of the protein imaging agent within the vehicle. Based on the imaging results of this multifunctional nanodrug, we could promptly adjust the tumor treatment regimens, thus improving the treatment flexibility for bladder cancer.

https://doi.org/10.1021/acsomega.2c03561
ACS Omega 2022, 7, 31299−31308

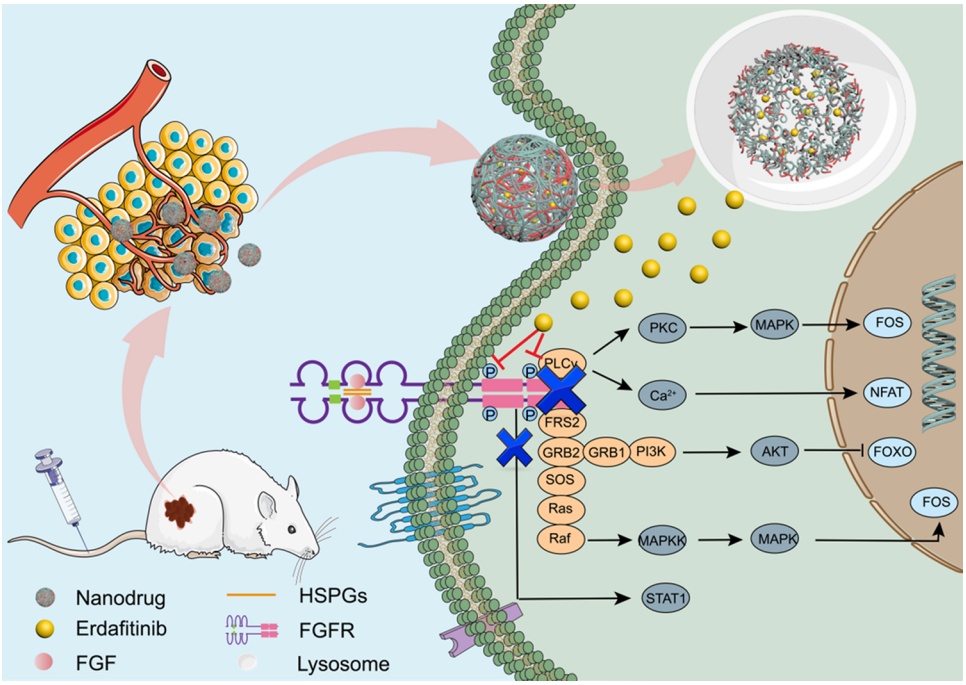

Figure 5. Illustration of the intrinsic therapeutic mechanism of the nanodrug. After intravenous administration, the nanodrug aggregated at the tumor location and was subsequently transferred to lysosomes. Erdafitinib was further released from the nanodrug into the cytoplasm, where it blocked the downstream signal pathways by inhibiting the phosphorylation of the kinase domain.

We further explored the intracellular distribution of the nanodrug. As shown in Figure S8, the PBS-treated T24 cell solely displayed the fluorescence of the cell membrane and lysosomes. However, a distinct blue fluorescence emerged after incubation with erdafitinib, and the fluorescence overlapped with that of the lysosome, indicating that erdafitinib was mainly distributed in lysosomes. Interestingly, this phenomenon also appeared in nanodrug-treated cells, indicating that the nanodrug mostly accumulated in the lysosomes after being transferred into the cells (Figure 4C).

On the basis of these findings, we proposed a possible mechanism underlying the treatment effects of such a nanodrug (Figure 5). The activation of FGFR signal pathways is triggered by the dimerization of the fibroblast growth factor (FGF)/FGFR/heparan sulfate proteoglycans (HSPG) ternary and the following phosphorylation of the intracellular kinase region.[39−41] Erdafitinib is reported to play an essential role in inhibiting the phosphorylation process, thus blocking the downstream signal pathways. In this work, the nanodrug penetrated the tumor tissue through the incomplete tumor vessel wall and was unable to re-enter the circulation because of the inadequate lymphatic system of the tumor tissue.[42] Therefore, more nanodrugs aggregated at the tumor location, and then they were endocytosed and transferred to the lysosomes. In the acidic environment of lysosomes, the electrostatic interaction was sustainably destroyed, and erdafitinib was then slowly released into the cytoplasm. Subsequently, erdafitinib effectively hindered the phosphorylation of the FGFR kinase domain, thus blocking the downstream FRS2, PLCγ, and STAT signal pathways.[40] As a result, the following tumor cell proliferation, migration, and angiogenesis were further inhibited.

CONCLUSIONS

In this work, we prepared a long-acting proteinaceous nanodrug through a simple self-assembly strategy, which displayed robust therapeutic effects as well as a superb fluorescence imaging capability for bladder tumors. The *in vivo* half-life and AUC of the nanodrug reached 14.4 h and 8.0 μg/mL·h, respectively, which were 8.3 times and 5.0 times higher than those of pure erdafitinib. Consequently, the dosage regimen was shortened from once a day to a total of three doses in 2 weeks. Even though the dose was reduced, the medium concentration of the long-lasting nanodrug also generated a comparable anti-tumor effect with a TGI of 69.1%. Strikingly, side effects of erdafitinib administration such as hyperphosphatemia were significantly alleviated in the nanodrug-treated mice models. In addition, the targeted-imaging capability of the nanodrug further increased the flexibility of tumor treatment because of its real-time surveillance of the therapeutic response. This study established a robust nanoplatform that not only afforded an effective strategy for simultaneous tumor suppression and surveillance but also significantly mitigated the side effects of erdafitinib. Thus, the development of our nanodrug broadens the clinical application of erdafitinib, providing a promising direction for the comprehensive treatment of bladder cancer.

EXPERIMENTAL SECTION

Materials. The expression vector and PEG-COOH were from our laboratory collection. *Escherichia coli* BLR(DE3) (Novagen) was used for protein production. Erdafitinib was purchased from Wuhan Yongcan Biotechnology Co. Ltd (Wuhan, China). Dimethyl sulfoxide (DMSO), calcein-AM, propidium iodide (PI), and 4% paraformaldehyde solution were bought from Aladdin (Shanghai, China). The Cell Counting Kit-8 (CCK-8) was provided by APExBIO Technology. Hematoxylin and Eosin (H&E), Ki67, trypsin−

https://doi.org/10.1021/acsomega.2c03561
ACS Omega 2022, 7, 31299−31308

EDTA solution, the Micro Blood Phosphorus Concentration Assay Kit, penicillin, and streptomycin were purchased from Solarbio Science & Technology (Beijing, China). The human bladder cancer cell line (T24 cells) was bought from Keygen Biotechnology (Nanjing, China). The human bladder cancer cell line (RT4 Cells) and McCoy' 5A medium were purchased from Procell life Science&Technology Co. Ltd. (Wuhan China). RPMI 1640 medium, phosphate-buffered saline (PBS), and fetal bovine serum (FBS) were provided by Gibco life technologies.

Expression and Purification of the Chimeric Protein. The bacterial inoculum was added to 100 mL of LB culture medium on a shaker at 220 rpm, 37 °C, for about 7 h until the OD600 reached 3−4. Then, the bacteria were transferred into 1 L of TB culture medium and kept shaking for 2 h. When the OD600 reached 0.6−0.8, isopropyl β-D-1-thiogalactopyranoside was added, and shaking was continued at 28.5 °C for 12 h. The cultured *E. coli* were harvested by centrifugation at 7000*g* for 10 min. The obtained bacteria were resuspended in a lysis buffer (50 mM sodium phosphate buffer, pH 8.0, 300 mM NaCl) and disrupted by a constant cell disrupter (Constant Systems LTD., Daventry, U.K.). After centrifuging, the recombinant protein was purified by Ni-sepharose chromatography, cation-exchange chromatography, and desalting. Sephadex S-100 molecular sieving chromatography was used to remove endotoxins, and the endotoxins in the purified protein products were characterized using the limulus amebocyte lysate (LAL) agent (Zhanjiang A&C Biological LTD, China). The endotoxin levels in protein samples were less than 5 EU/kg. The obtained solvent was lyophilized and stored at −80 °C before use.

SDS-PAGE Analysis. Protein samples were boiled, centrifuged, and loaded on 12% sodium dodecyl sulfate−polyacrylamide (SDS-PAGE) gels together with a prestained protein marker (Blue Plus II, TransGen). Afterward, gels were stained with the Coomassie staining solution (40% methanol, 10% glacial acetic acid, and 1 g/L Brilliant Blue R250).

Matrix-Assisted Laser Desorption/Ionization Time-of-Flight (MALDI-TOF) Mass Spectrometry. The purified protein sample was prepared at a concentration of 1 mg/mL using Milli-Q water as the solvent, and this test was carried out using autoflexIII MALDI-TOF/TOF, Bruker.

Synthesis of PEG-COOH. PEG-COOH was prepared according to the reported method.[18] First of all, 1.0 mmol of PEG-diol and 0.33 mmol of boric acid were mixed and stirred at 70 °C for 5 h under a pressure of 1.33 kPa. The formed polyethylene glycol monoborate was further mixed with 3.48 mmol of *p*-tuloenesulfonic acid and 1.01 mmol of succinic anhydride; the mixture was stirred at 130 °C for 15 h under a pressure of 1.33 kPa. The reaction mixture was adjusted to pH 7 with 10% sodium carbonate aqueous solution and stirred at 100 °C for 3 h to hydrolyze the polyethylene glycol monoborate. The molecular weight of PEG-COOH was 5000, and each molecule shares one carboxylic group. The synthetic route is presented in Figure S9.

Fabrication of the Nanodrug. For animal injection purposes, mIFP-K72 and PEG-COOH were dissolved separately in PBS (pH 7.4). At a charge ratio of 1:1, PEG-COOH and mIFP-K72 were fully mixed, and erdafitinib was added afterward. The mixture was stirred at 37 °C for 1 h. To separate free PEG-COOH and free polypeptide molecules from the nanodrug, gravity-driven chromatography using a NAP-10 column (General Electric Company) was performed at room temperature and under atmospheric pressure. The fraction of the complexed nanodrug was collected and concentrated by ultrafiltration. When the nanodrug was used for analyses by transmission electron microscopy or DLS, the solvent was replaced with Milli-Q water rather than PBS. At the beginning of the nanodrug formulation, we added 7.1 mg of erdafitinib into the solution. The final concentration of encapsulated erdafitinib was 3.1 mg/mL through the precise assembly approach. The loading efficiency and encapsulation efficiency were determined by the following equation

$$\text{loading efficiency} = m_{\text{encapsulatederdafitinib}}/(m_{\text{encapsulatederdafitinib}} + m_{\text{mIFP-K72}} + m_{\text{PEG-COOH}}) \times 100\%$$

$$\text{encapsulation efficiency} = m_{\text{encapsulatederdafitinib}}/m_{\text{totalerdafitinib}} \times 100\%$$

Transmission Electron Microscopy (TEM). Transmission electron microscopy (TEM) was carried out using a JEOL-2010 transmission electron microscope (JEOL Co., Japan) with an acceleration voltage of 200 kV. The samples were coated on a carbon film and dried at 60 °C overnight.

Dynamic Light Scattering. The hydrodynamic size was measured using a Zetasizer Nano ZS (Malvern Instruments Ltd, U.K.). The samples were prepared using Milli-Q water.

***In Vitro* Cytotoxicity Assay.** The *in vitro* cytotoxicity assay of medicines was performed using a CCK-8 kit. T24 and RT4 cells were seeded into 96-well plates at densities of 3×10^3 and 5×10^3 per well and incubated for 24 h, respectively. Then, a series of concentrations of different drugs was applied to the corresponding groups. After incubation for 72 h, CCK-8 was added to each well at a final concentration of 10%. After another incubation of 1.5 h, the absorbance of the medium was measured at 450 nm. The concentrations of erdafitinib were kept identical in the erdafitinib and nanodrug group, and the concentration of the vehicle was determined by the corresponding concentration of the nanodrug. The IC50 was calculated using GraphPad Prism 8.3.0.

$$\text{cell viability}(\%) = (\text{mean OD}_{\text{sample}} - \text{mean OD}_{\text{blank}})/(\text{mean OD}_{\text{control}} - \text{mean OD}_{\text{blank}}) \times 100\%$$

***In Vitro* Medicine Distribution.** We performed confocal laser scanning microscopy (C2 Nikon, Japan) to investigate the intracellular distribution of the medicine. T24 cells (3×10^3) were seeded into 96-well plates and incubated for 24 h. Then, 20 μmol/L erdafitinib or nanodrug was added, followed by 8 h of incubation. Then, the medium was removed, and the cells were washed three times. Dil and Lysosome-Tracker were added to stain the cell membrane and lysosomes. The cell membrane, lysosomes, and erdafitinib were stained in red, green, and blue on excitation with 561, 488, and 408 nm lasers, respectively.

Live/Dead Staining Assay. RT4/T24 cells (5×10^4) were seeded into six-well plates. After 24 h of incubation, 20 μmol/L erdafitinib or nanodrug was added and cultivated for 24 and 48 h for RT4 and T24 cells, respectively. The medium was then removed, and the cells were washed with PBS three times. Subsequently, 200 μL of the buffer containing calcein-AM and

https://doi.org/10.1021/acsomega.2c03561
ACS Omega 2022, 7, 31299−31308

PI was added to each well and incubated for 30 min at 37 °C in darkness. After washing with PBS three times, the fluorescence images of RT4/T24 cells were observed using a confocal laser scanning microscope (C2 Nikon, Japan).

***In Vivo* Anti-Tumor Studies.** All animal experiments were conducted in compliance with the Animal Management Rules of the Ministry of Health of the People's Republic of China and were carried out with the approval of the Institutional Animal Care and Use Committee of the Animal Experiment Center of Jilin University (Changchun, China). Five-week-old female BALB/c nude mice were prepared for *in vivo* anti-tumor studies. We subcutaneously injected 5×10^6 RT4 cells (200 μL of PBS) in the right hind leg of nude mice. Once the tumor volume reached 100 mm^3, the nude mice were randomly divided into six groups. The nanodrug, PBS, and vehicle were intravenously injected via the tail vein on days 1, 4, and 7 into the corresponding groups. In contrast, models in the erdafitinib group were given an erdafitinib/Milli-Q water suspension (25 mg/kg) orally once a day. During the observation period of 2 weeks, the tumor volumes and body weights were recorded every 3 days. The length and width of tumors were measured using a vernier caliper. After the entire observation for 14 days, all of the RT4 tumor-bearing nude mice were sacrificed and dissected; tumors were collected for further H&E and Ki67 staining.

$$\text{tumor volumes} = \text{length} \times \text{width}^2/2$$

Immunohistochemistry and H&E Staining. All of the excised tumors for staining were first fixed with 4% paraformaldehyde solution. After that, the samples were dehydrated using grades of ethanol (70, 80, 90, 95, and 100%). Lastly, the samples were impregnated with molten paraffin wax, embedded, and cut into blocks. The organ or tumor sections were cut into 2−4 μm thickness and mounted on glass slides. Then, the hematoxylin and eosin (H&E) staining and immunohistochemistry staining of Ki67 were performed. Images of stained sections were obtained using an optical microscope (Nikon, Japan). The quantitative analysis of Ki67 expression was carried out using Image-Pro Plus.

Evaluation of *In Vivo* Pharmacokinetic Parameters of the Nanodrug. For the evaluation of pharmacokinetic parameters, the nanodrug was intravenously injected via the tail vein into female BALB/c mice. At 0.5, 1, 1.5, 2, 4, 8, and 12 h after injection, blood samples were collected via the facial vein. After centrifugation (3000 rpm, 15 min), the obtained serum was fully mixed with acetonitrile, and the precipitate was removed after centrifugation (12 000 rpm, 15 min). The supernatant was dried at 60 °C overnight and redissolved in methanol. The concentration of erdafitinib was detected by high-performance liquid chromatography (HPLC) as described in the literature.[36]

***In Vivo* and *In Vitro* Imaging of Tumor Xenografts.** The tumor xenograft mice models were prepared using BALB/c-nude mice. The mice were imaged by the Maestro EX fluorescence imaging system (Cambridge Research and Instrumentation, CRi) at 16 h after injection. After imaging, mice were sacrificed by cervical dislocation, and tumors were removed. Then, tumors were immediately imaged *ex vivo*. Settings for fluorescence measurements were excitation at 665 nm and emission at 710 nm.

■ ASSOCIATED CONTENT

Supporting Information

The Supporting Information is available free of charge at https://pubs.acs.org/doi/10.1021/acsomega.2c03561.

Additional characterization results concerning the SDS-PAGE analysis, images of the assembly process, TEM images, DLS analysis, *in vitro* cytotoxicity assay, live/dead staining, and *in vitro* biodistribution of PBS/erdafitinib (PDF)

■ AUTHOR INFORMATION

Corresponding Authors

Xinquan Gu − *Department of Urology, China-Japan Union Hospital of Jilin University, Changchun 130033, China*; Email: guxq@jlu.edu.cn

Fuquan Jiang − *Department of Urology, China-Japan Union Hospital of Jilin University, Changchun 130033, China*; Email: jiangfq@jlu.edu.cn

Yao Sun − *Department of Chemistry, Tsinghua University, Beijing 100084, China*; Email: yaosun@mail.tsinghua.edu.cn

Jingjing Li − *State Key Laboratory of Rare Earth Resource Utilization, Changchun Institute of Applied Chemistry, Chinese Academy of Sciences, Changchun 130022, China*; orcid.org/0000-0002-7526-5308; Email: jjingli@ciac.ac.cn

Authors

Lai Zhao − *Department of Urology, China-Japan Union Hospital of Jilin University, Changchun 130033, China; State Key Laboratory of Rare Earth Resource Utilization, Changchun Institute of Applied Chemistry, Chinese Academy of Sciences, Changchun 130022, China*

Bo Li − *State Key Laboratory of Rare Earth Resource Utilization, Changchun Institute of Applied Chemistry, Chinese Academy of Sciences, Changchun 130022, China; Department of Chemistry, Tsinghua University, Beijing 100084, China*

Shuang Lu − *State Key Laboratory of Rare Earth Resource Utilization, Changchun Institute of Applied Chemistry, Chinese Academy of Sciences, Changchun 130022, China*

Fan Wang − *State Key Laboratory of Rare Earth Resource Utilization, Changchun Institute of Applied Chemistry, Chinese Academy of Sciences, Changchun 130022, China*

Kai Liu − *State Key Laboratory of Rare Earth Resource Utilization, Changchun Institute of Applied Chemistry, Chinese Academy of Sciences, Changchun 130022, China; Department of Chemistry, Tsinghua University, Beijing 100084, China*; orcid.org/0000-0003-0878-5191

Complete contact information is available at: https://pubs.acs.org/10.1021/acsomega.2c03561

Author Contributions

L.Z. performed/analyzed the experiments and conceived the manuscript; B.L. and S.L. helped with the animal experiments; F.W. and K.L. contributed to the designing of experiments; X.G., F.J., Y.S., and J.L. provided guidance for the experiments and the revision of the manuscript.

Notes

The authors declare no competing financial interest.

https://doi.org/10.1021/acsomega.2c03561
ACS Omega 2022, 7, 31299−31308

■ ACKNOWLEDGMENTS

This study was supported by the National Key R&D Program of China (2020YFA0908900, 2021YFB3502300, and 2021YFF0701800), the National Natural Science Foundation of China (Grant Nos. 21877104, 21834007, 22020102003, 22107097, 21907088, and 22125701), and the Youth Innovation Promotion Association of CAS (Grant Nos. 2020228, 2021226).

■ REFERENCES

(1) Saginala, K.; Barsouk, A.; Aluru, J. S.; Rawla, P.; Padala, S. A.; Barsouk, A. Epidemiology of Bladder Cancer. *Med. Sci.* **2020**, *8*, 15.
(2) Sung, H.; Ferlay, J.; Siegel, R. L.; Laversanne, M.; Soerjomataram, I.; Jemal, A.; Bray, F. Global Cancer Statistics 2020: GLOBOCAN Estimates of Incidence and Mortality Worldwide for 36 Cancers in 185 Countries. *Ca-Cancer J. Clin.* **2021**, *71*, 209−249.
(3) Jain, P.; Kathuria, H.; Momin, M. Clinical Therapies and Nano Drug Delivery Systems for Urinary Bladder Cancer. *Pharmacol. Ther.* **2021**, *226*, No. 107871.
(4) Tran, L.; Xiao, J.-F.; Agarwal, N.; Duex, J. E.; Theodorescu, D. Advances in Bladder Cancer Biology and Therapy. *Nat. Rev. Cancer* **2021**, *21*, 104−121.
(5) Markham, A. Erdafitinib: First Global Approval. *Drugs* **2019**, *79*, 1017−1021.
(6) Perera, T. P. S.; Jovcheva, E.; Mevellec, L.; Vialard, J.; De Lange, D.; Verhulst, T.; Paulussen, C.; Van De Ven, K.; King, P.; Freyne, E.; Rees, D. C.; Squires, M.; Saxty, G.; Page, M.; Murray, C. W.; Gilissen, R.; Ward, G.; Thompson, N. T.; Newell, D. R.; Cheng, N.; Xie, L.; Yang, J.; Platero, S. J.; Karkera, J. D.; Moy, C.; Angibaud, P.; Laquerre, S.; Lorenzi, M. V. Discovery & Pharmacological Characterization of JNJ-42756493 (Erdafitinib), a Functionally Selective Small-Molecule FGFR Family Inhibitor. *Mol. Cancer Ther.* **2017**, *16*, 1010−1020.
(7) Loriot, Y.; Necchi, A.; Park, S. H.; Garcia-Donas, J.; Huddart, R.; Burgess, E.; Fleming, M.; Rezazadeh, A.; Mellado, B.; Varlamov, S.; Joshi, M.; Duran, I.; Tagawa, S. T.; Zakharia, Y.; Zhong, B.; Stuyckens, K.; Santiago-Walker, A.; De Porre, P.; O'Hagan, A.; Avadhani, A.; Siefker-Radtke, A. O. Erdafitinib in Locally Advanced or Metastatic Urothelial Carcinoma. *N. Engl. J. Med.* **2019**, *381*, 338−348.
(8) Nishina, T.; Takahashi, S.; Iwasawa, R.; Noguchi, H.; Aoki, M.; Doi, T. Safety, Pharmacokinetic, and Pharmacodynamics of Erdafitinib, a Pan-Fibroblast Growth Factor Receptor (FGFR) Tyrosine Kinase Inhibitor, in Patients with Advanced or Refractory Solid Tumors. *Invest. New Drugs* **2018**, *36*, 424−434.
(9) Liu, D.; Wang, C.; Yang, J.; An, Y.; Yang, R.; Teng, G. CRGDK-Functionalized PAMAM-Based Drug-Delivery System with High Permeability. *ACS Omega* **2020**, *5*, 9316−9323.
(10) Wang, S.; Zhang, H.; Li, B.; Chen, C.; Ren, T.; Huang, Y.; Liu, K.; Li, J.; Guo, W. Knockdown of a Specific Circular Non-Coding RNA Significantly Suppresses Osteosarcoma Progression *Engineering* 2022, DOI: 10.1016/j.eng.2021.12.007.
(11) Li, J.; Sun, Y.; Liang, Y.; Ma, J.; Li, B.; Ma, C.; Tanzi, R. E.; Zhang, H.; Liu, K.; Zhang, C. Extracellular Elastin Molecule Modulates Alzheimer's Aβ Dynamics In Vitro and In Vivo by Affecting Microglial Activities. *CCS Chem.* **2021**, *3*, 1830−1837.
(12) Yang, N.; Cao, C.; Li, H.; Hong, Y.; Cai, Y.; Song, X.; Wang, W.; Mou, X.; Dong, X. Polymer-Based Therapeutic Nanoagents for Photothermal-Enhanced Combination Cancer Therapy. *Small Struct.* **2021**, *2*, No. 2100110.
(13) Ang, M. J. Y.; Chan, S. Y.; Goh, Y.-Y.; Luo, Z.; Lau, J. W.; Liu, X. Emerging Strategies in Developing Multifunctional Nanomaterials for Cancer Nanotheranostics. *Adv. Drug Delivery Rev.* **2021**, *178*, No. 113907.
(14) Wang, J.; Li, Y.; Nie, G.; Zhao, Y. Precise Design of Nanomedicines: Perspectives for Cancer Treatment. *Natl. Sci. Rev.* **2019**, *6*, 1107−1110.
(15) Ma, C.; Li, B.; Zhang, J.; Sun, Y.; Li, J.; Zhou, H.; Shen, J.; Gu, R.; Qian, J.; Fan, C.; Zhang, H.; Liu, K. Significantly Improving the Bioefficacy for Rheumatoid Arthritis with Supramolecular Nanoformulations. *Adv. Mater.* **2021**, *33*, No. 2100098.
(16) Wang, S.; Li, B.; Zhang, H.; Chen, J.; Sun, X.; Xu, J.; Ren, T.; Zhang, Y.; Ma, C.; Guo, W.; Liu, K. Improving Bioavailability of Hydrophobic Prodrugs through Supramolecular Nanocarriers Based on Recombinant Proteins for Osteosarcoma Treatment. *Angew. Chem., Int. Ed.* **2021**, *60*, 11252−11256.
(17) Zhang, J.; Sun, Y.; Qu, Q.; Li, B.; Zhang, L.; Gu, R.; Zuo, J.; Wei, W.; Ma, C.; Liu, L.; Liu, K.; Li, J.; Zhang, H. Engineering Non-Covalently Assembled Protein Nanoparticles for Long-Acting Gouty Arthritis Therapy. *J. Mater. Chem. B* **2021**, *9*, 9923−9931.
(18) Li, J.; Li, B.; Sun, J.; Ma, C.; Wan, S.; Li, Y.; Göstl, R.; Herrmann, A.; Liu, K.; Zhang, H. Engineered Near-Infrared Fluorescent Protein Assemblies for Robust Bioimaging and Therapeutic Applications. *Adv. Mater.* **2020**, *32*, No. 2000964.
(19) Ong, W. K.; Yao, X.; Jana, D.; Li, M.; Zhao, Y.; Luo, Z. Efficient Production of Reactive Oxygen Species from Fe 3 O 4 /ZnPC Coloaded Nanoreactor for Cancer Therapeutics In Vivo. *Small Struct.* **2020**, *1*, No. 2000065.
(20) Xu, Y.; Zhao, M.; Zhou, Y.; Wang, J.; Li, M.; Li, F.; Lv, W.; Liu, S.; Zhao, Q. Rational Design of Near-Infrared Aza-Platinum-Dipyrromethene-Based Nanophototherapy Agent with Multistage Enhancement for Synergistic Antitumor Therapeutics. *Small Struct.* **2021**, *2*, No. 2100094.
(21) Suárez-García, S.; Solórzano, R.; Novio, F.; Alibés, R.; Busqué, F.; Ruiz-Molina, D. Coordination Polymers Nanoparticles for Bioimaging. *Coord. Chem. Rev.* **2021**, *432*, No. 213716.
(22) Boisselier, E.; Astruc, D. Gold Nanoparticles in Nanomedicine: Preparations, Imaging, Diagnostics, Therapies and Toxicity. *Chem. Soc. Rev.* **2009**, *38*, 1759.
(23) Zhao, K.; Sun, J.; Wang, F.; Song, A.; Liu, K.; Zhang, H. Lanthanide-Based Photothermal Materials: Fabrication and Biomedical Applications. *ACS Appl. Bio Mater.* **2020**, *3*, 3975−3986.
(24) Shao, B.; Wan, S.; Yang, C.; Shen, J.; Li, Y.; You, H.; Chen, D.; Fan, C.; Liu, K.; Zhang, H. Engineered Anisotropic Fluids of Rare-Earth Nanomaterials. *Angew. Chem., Int. Ed.* **2020**, *59*, 18213−18217.
(25) Hassan, S.; Prakash, G.; Bal Ozturk, A.; Saghazadeh, S.; Farhan Sohail, M.; Seo, J.; Remzi Dokmeci, M.; Zhang, Y. S.; Khademhosseini, A. Evolution and Clinical Translation of Drug Delivery Nanomaterials. *Nano Today* **2017**, *15*, 91−106.
(26) Cai, Y.; Chen, X.; Si, J.; Mou, X.; Dong, X. All-in-One Nanomedicine: Multifunctional Single-Component Nanoparticles for Cancer Theranostics. *Small* **2021**, *17*, No. 2103072.
(27) Younis, M. A.; Tawfeek, H. M.; Abdellatif, A. A. H.; Abdel-Aleem, J. A.; Harashima, H. Clinical Translation of Nanomedicines: Challenges, Opportunities, and Keys. *Adv. Drug Delivery Rev.* **2022**, *181*, No. 114083.
(28) Kumar, R.; Dalvi, S. V.; Siril, P. F. Nanoparticle-Based Drugs and Formulations: Current Status and Emerging Applications. *ACS Appl. Nano Mater.* **2020**, *3*, 4944−4961.
(29) Ma, C.; Sun, J.; Li, B.; Feng, Y.; Sun, Y.; Xiang, L.; Wu, B.; Xiao, L.; Liu, B.; Petrovskii, V. S.; Bin, Liu.; Zhang, J.; Wang, Z.; Li, H.; Zhang, L.; Li, J.; Wang, F.; Göstl, R.; Potemkin, I. I.; Chen, D.; Zeng, H.; Zhang, H.; Liu, K.; Herrmann, A. Ultra-Strong Bio-Glue from Genetically Engineered Polypeptides. *Nat. Commun.* **2021**, *12*, No. 3613.
(30) Xiao, L.; Wang, Z.; Sun, Y.; Li, B.; Wu, B.; Ma, C.; Petrovskii, V. S.; Gu, X.; Chen, D.; Potemkin, I. I.; Herrmann, A.; Zhang, H.; Liu, K. An Artificial Phase-Transitional Underwater Bioglue with Robust and Switchable Adhesion Performance. *Angew. Chem., Int. Ed.* **2021**, *60*, 12082−12089.
(31) Chell, V.; Balmanno, K.; Little, A. S.; Wilson, M.; Andrews, S.; Blockley, L.; Hampson, M.; Gavine, P. R.; Cook, S. J. Tumour Cell Responses to New Fibroblast Growth Factor Receptor Tyrosine Kinase Inhibitors and Identification of a Gatekeeper Mutation in FGFR3 as a Mechanism of Acquired Resistance. *Oncogene* **2013**, *32*, 3059−3070.

https://doi.org/10.1021/acsomega.2c03561
ACS Omega 2022, 7, 31299−31308

(32) Cheng, T.; Roth, B.; Choi, W.; Black, P. C.; Dinney, C.; McConkey, D. J. Fibroblast Growth Factor Receptors-1 and -3 Play Distinct Roles in the Regulation of Bladder Cancer Growth and Metastasis: Implications for Therapeutic Targeting. *PLoS One* **2013**, *8*, No. e57284.
(33) Luo, Y.; Ju, L.; Wang, G.; Chen, C.; Wang, Y.; Chen, L.; Zhang, Y.; Xiao, Y.; Wang, X. Comprehensive Genomic Profiling of Urothelial Carcinoma Cell Lines Reveals Hidden Research Bias and Caveats. *Clin. Transl. Med.* **2020**, *10*, 294−296.
(34) Abánades Lázaro, I.; Haddad, S.; Sacca, S.; Orellana-Tavra, C.; Fairen-Jimenez, D.; Forgan, R. S. Selective Surface PEGylation of UiO-66 Nanoparticles for Enhanced Stability, Cell Uptake, and PH-Responsive Drug Delivery. *Chem* **2017**, *2*, 561−578.
(35) You, X.; Wang, L.; Wang, L.; Wu, J. Rebirth of Aspirin Synthesis By-Product: Prickly Poly(Salicylic Acid) Nanoparticles as Self-Anticancer Drug Carrier. *Adv. Funct. Mater.* **2021**, *31*, No. 2100805.
(36) Elawady, T.; Khedr, A.; El-Enany, N.; Belal, F. HPLC-UV Determination of Erdafitinib in Mouse Plasma and Its Application to Pharmacokinetic Studies. *J. Chromatogr. B: Anal. Technol. Biomed. Life Sci.* **2021**, *1171*, No. 122629.
(37) Shi, D.; Beasock, D.; Fessler, A.; Szebeni, J.; Ljubimova, J. Y.; Afonin, K. A.; Dobrovolskaia, M. A. To PEGylate or Not to PEGylate: Immunological Properties of Nanomedicine's Most Popular Component, Polyethylene Glycol and Its Alternatives. *Adv. Drug Delivery Rev.* **2022**, *180*, No. 114079.
(38) Dosne, A.; Valade, E.; Stuyckens, K.; De Porre, P.; Avadhani, A.; O'Hagan, A.; Li, L. Y.; Ouellet, D.; Faelens, R.; Leirens, Q.; Poggesi, I.; Perez Ruixo, J. J. Erdafitinib's Effect on Serum Phosphate Justifies Its Pharmacodynamically Guided Dosing in Patients with Cancer. *CPT: Pharmacometrics Syst. Pharmacol.* **2022**, *11*, 569−580.
(39) Cheng, W.; Wang, M.; Tian, X.; Zhang, X. An Overview of the Binding Models of FGFR Tyrosine Kinases in Complex with Small Molecule Inhibitors. *Eur. J. Med. Chem.* **2017**, *126*, 476−490.
(40) Goetz, R.; Mohammadi, M. Exploring Mechanisms of FGF Signalling through the Lens of Structural Biology. *Nat. Rev. Mol. Cell Biol.* **2013**, *14*, 166−180.
(41) Xie, Y.; Su, N.; Yang, J.; Tan, Q.; Huang, S.; Jin, M.; Ni, Z.; Zhang, B.; Zhang, D.; Luo, F.; Chen, H.; Sun, X.; Feng, J. Q.; Qi, H.; Chen, L. FGF/FGFR Signaling in Health and Disease. *Signal Transduction Targeted Ther.* **2020**, *5*, No. 181.
(42) Golombek, S. K.; May, J.-N.; Theek, B.; Appold, L.; Drude, N.; Kiessling, F.; Lammers, T. Tumor Targeting via EPR: Strategies to Enhance Patient Responses. *Adv. Drug Delivery Rev.* **2018**, *130*, 17−38.

https://doi.org/10.1021/acsomega.2c03561
ACS Omega 2022, 7, 31299−31308